Applied Physics Letters

Grain boundary segregation and carbide precipitation in heat treated niobium superconducting radio frequency cavities

Cite as: Appl. Phys. Lett. **119**, 194102 (2021); https://doi.org/10.1063/5.0063379
Submitted: 14 July 2021 • Accepted: 26 October 2021 • Published Online: 09 November 2021

A. Dangwal Pandey, T. F. Keller, M. Wenskat, et al.

AIP Publishing

Applied Physics Letters ARTICLE scitation.org/journal/apl

Grain boundary segregation and carbide precipitation in heat treated niobium superconducting radio frequency cavities

Cite as: Appl. Phys. Lett. **119**, 194102 (2021); doi: 10.1063/5.0063379
Submitted: 14 July 2021 · Accepted: 26 October 2021 ·
Published Online: 9 November 2021

A. Dangwal Pandey,[1,a)] T. F. Keller,[1,2] M. Wenskat,[2] A. Jeromin,[1] S. Kulkarni,[1] H. Noei,[1] V. Vonk,[1] W. Hillert,[2,3] D. Reschke,[3] N. Walker,[3] H. Weise,[3] and A. Stierle[1,2]

AFFILIATIONS

[1]Centre for X-ray and Nano Science (CXNS), Deutsches Elektronen-Synchrotron, 22607 Hamburg, Germany
[2]Fachbereich Physik, Universität Hamburg, 22607 Hamburg, Germany
[3]Deutsches Elektronen-Synchrotron, 22607 Hamburg, Germany

[a)]Author to whom correspondence should be addressed: arti.pandey@desy.de

ABSTRACT

A fundamental understanding of superconducting radio frequency Nb cavity processing is necessary to achieve the desired improvement in their performance, which is needed for further upgrades of modern particle accelerators. To recognize the physical processes behind the losses in the accelerator modules, it is required to address not only the observed improvements but also the degradation occurring after different surface treatments. Here, we report on microscopic and spectroscopic studies of several cutouts from an extremely well performing cavity, which showed a systematic degradation after modified surface treatments and annealing conditions. Our results suggest that an abundance of low-angle grain boundaries surrounding the small sized grains can be related to the local superconductivity breakdown at high accelerating field gradients. Losses due to grain boundary segregated carbides are discussed to being most dominant and to leading to an anomalous Q-degradation of the whole cavity starting at low fields.

Superconducting radio frequency (SRF) Niobium cavities are one of the basic building blocks for modern highly brilliant light sources like x-ray free electron lasers (XFELs), being operated at a very high accelerating electric field gradient (E_{acc}) with high quality-factors ($Q \propto 1/$ surface resistance). Over eight hundred Nb cavities installed in the European XFEL are being operated with an average Q-value higher than 1×10^{10} and maximum E_{acc} of $\approx$30 MV/m.[1] SRF Nb with high Q is also of high interest to quantum computing,[2,3] with a possibility of increasing qubit lifetime.[4,5]

For the European XFEL cavity production, a Nb surface preparation recipe was used, including a high vacuum annealing at 800 °C, material removal by chemical polishing, and 120 °C bake in vacuum before RF tests.[6] A recently developed heat treatment of SRF Nb cavities in nitrogen atmosphere, termed as "nitrogen-infusion,"[7] is reported to result appreciably higher Q-values (2×10^{10}) at high $E_{acc} \approx 45$ MV/m. In this case, high vacuum annealing of cavities is directly followed by 120 °C bake in a nitrogen atmosphere. Excluding the material removal step at the end of the overall surface treatment, using HF and H_2SO_4, avoids new intake of hydrogen from the chemical reaction. An increased N-concentration in the near-surface regions of the samples cut out from the N-infused cavities was reported by means of secondary ion mass spectroscopy.[7–9] H and other light elements, such as C, N, and O, are present in Nb lattice as interstitial impurities. During the cavity cool-down to liquid-He temperatures, surface segregation of hydrogen leads to precipitation of niobium hydrides on the cavity surface, which are assumed to be responsible for an exponential drop in Q at high $E_{acc.}$[10–13] Nitrogen is known to be a trapping center for H-interstitial and, thus, can suppress the precipitation of the hydrides.[14–17] However, reproduction of the N-infusion of SRF cavities leading to an extra-ordinary high Q remains a big challenge for many laboratories.[18–20] Specifically, the role of omnipresent Nb carbide formation even under best high vacuum conditions for the cavity performance is unclear.

In this paper, we correlate the local structure and chemical composition of cutouts of a Nb cavity to its SRF performance. This cavity was one among three very well performing cavities fabricated during the European XFEL production phase, which were degraded in a similar manner under preparation conditions.[18] The cutouts were taken

from the locations identified as the origin of the superconductivity breakdown (quench regions) as well as those exhibiting minimum RF and thermal losses (cold regions).We will show that different types of losses observed can be related to the enhanced grain boundary (GB) carbide segregation and excess of very small grains containing low-angle GBs in the quench regions.

A polycrystalline, TESLA shaped Nb cavity[21] was prepared after more than 180 μm material removal and applying the following surface preparation steps: (I) annealing at 800 °C for 3 h in high vacuum, 40 μm electropolishing (EP), and 120 °C bake for 48 h in vacuum; (II) annealing at 800 °C for 3 h followed by 120 °C bake for 48 h in high vacuum, and (III) repetition of II. Quench locations were identified by second sound measurements[22,23] during the cavity tests; magnetic field (B) mapping and temperature (T) mapping of the cavity surface were also performed;[24] and the cavity was cut after treatment (III). More details on the cavity and cutouts can be found elsewhere.[18]

The resulting cavity performance after each treatment is given in Fig. 1(a) in the form of Q vs E_{acc} plots at 2 K. A sketch of the cavity shown in the inset of Fig. 1(a) represents the positions of the here studied cavity cutouts. Very high Q values (2×10^{10}) are observed up to a high accelerating field gradient of 33 MV/m after the treatment I, where the corresponding quench region (#4) lies far below the equator. Treatment II preserved high Q-values but limited the maximum E_{acc} to 27 MV/m, with a change in the quench position (#2) to the equator of the cavity. After the treatment III, a completely different type of Q degradation—decreasing exponentially with E_{acc}—was observed. No quench occurred in the last RF test, and the cavity was limited by the input power. Such a type of Q-degradation has been reported for: (i) non-annealed cavities[11,25] and (ii) cavities with Ti polluted GBs.[26,27] The cavities in the former case were cured after annealing to 750 –800 °C to facilitate most of the hydrogen to degas. In our case, cavities were annealed and no Ti contamination was detected by means of energy dispersive x-ray analysis (EDX). X-ray photoelectron spectroscopy (XPS) was employed to reveal the chemical composition of the surface layer on the different spots ($200 \times 200\ \mu m^2$ lateral resolution).[28] High resolution Nb 3d line profiles of the cold region (#1) and the quench region (#2) are shown in Fig. 1(b). The deconvoluted peaks confirm the niobium oxide phases: Nb_2O_5, NbO_2, NbO, and $Nb_xO (x < 1)$ with $3d_{5/2}$ orbital positions at 207.5, 206, 204, and 202.7 eV, respectively, on the Nb surface.[29–31] Higher intensity at 202.7 eV for the quench region could also be assigned to niobium-subcarbide Nb_2C.[32] The C 1s and O 1s spectra on cold and quench spots do not differ much due to a major contribution from the adventitious carbon and surface oxide layers grown on the cavity surface due its exposure to the atmosphere[33] after each heat treatment. To confirm the surface layer structure, we exploited electron back-scattered diffraction (EBSD) complementary to scanning electron microscope (SEM), which generates crystal orientation images based on automated crystal orientation indexation of so-called Kikuchi pattern[34] arising from multiple electron Bragg-reflection.

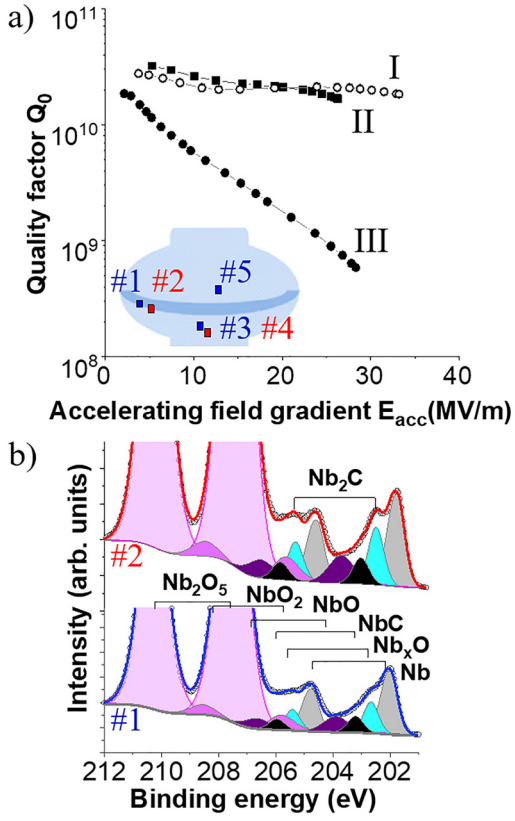

FIG. 1. (a) Q vs E_{acc} curves at 2 K of the SRF Nb cavity 1DE16 after (I) 800 °C/3 h + 40 μm EP + 120 °C/48 h, (II) annealing at 800 °C/3 h + 120 °C/48 h, and (III) again 800° C/3 h + 120 °C/48 h. Inset: Sketch of the cavity with the dark gray line representing the welding zone, marked squares represent the location of the cavity cuts: in blue for cold regions #1, #3, and #5, and in red for quench regions #2 and #4; (b) zoomed-in view of deconvoluted Nb 3d photoelectron spectra on cuts #1(blue) and #2(red), plotted with a vertical offset.

Large area EBSD maps on cold (#1) and quench (#2) regions are given in Figs. 2(a) and 2(b), respectively, which depict highly elongated Nb grains at the welding zone of the cavity, resulting from the fabrication. No appreciable difference in the Nb grain size distribution is noticed between both areas. However, the topography of the GBs shows marked dissimilarities, as shown in Figs. 2(c) and 2(d). EBSD maps confirm a large segregation of carbides, crystallizing in the α-Nb_2C phase, all along the GBs lying on the quench region—as shown in Figs. 2(d) and 2(f). In the cold region, GB carbide segregation is comparatively less and precipitates are too small to be detected in EBSD maps [Figs. 2(c) and 2(e)]. Triangular carbide precipitates are observed on all Nb grains by means of SEM; their occurrence and size distribution depends on the Nb grain orientation. For example, precipitates on Nb(223) lie at a larger distance to the GB when compared to those on the neighboring grains [Fig. 2(d)]. Big precipitates of size up to ~650 nm [Fig. 2(g)] are found on the quench region (#2), after treatment III. However, precipitates of dimension up to ~200 nm were observed on a single crystal Nb(221) sample co-treated with the cavity in treatment II (Fig. S1), suggesting smaller carbide growth during that temperature cycle. The electrical resistance of non-superconducting carbides[35] would lead to a local joule heating. Therefore, carbides when present in excess on the surface might become a source for a quench of the SRF Nb cavity.

An orthorhombic crystal structure of α-Nb_2C phase was detected for the precipitates as well as in the GB segregated carbides, with lattice constants a, b, c of 10.92, 4.97, and 3.09 Å, respectively, and $\alpha = \beta = \gamma = 90°$.[36] α-Nb_2C is one of three polymorphs of Nb

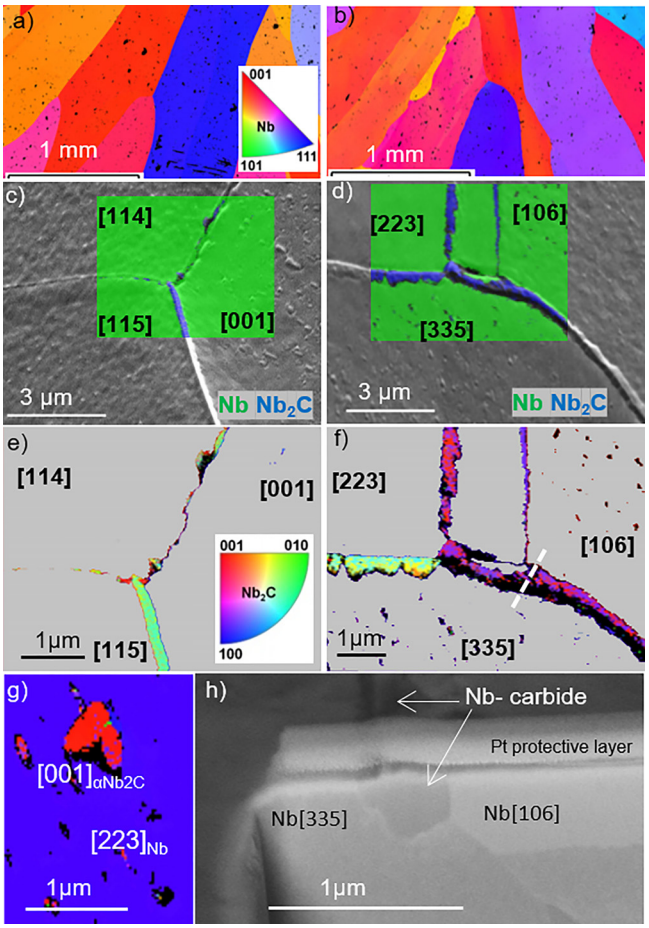

FIG. 2. On the cold region #1 and quench region #2 in left and right, respectively, for a–f: Nb grain orientation maps [(a), (b)], with inverse pole figure for bcc Nb [inset of (a)]; SEM images with Nb and Nb_2C phase identification overlay over the GB area [(c), (d)]; Nb_2C orientation maps in color [(e), (f)] with inverse pole figure for orthorhombic Nb_2C (inset of e); out-of-plane orientation maps of the carbide precipitates on Nb(223) grain (g); and FIB-milled cross section (h) along the dashed line in (f).

carbide, transforming to two hexagonal phases: β above 1200 °C and γ above 2500 °C.[36,37] The crystallographic orientation relationship of orthorhombic Nb_2C to bcc Nb lattice is observed to be as follows: $[103]\alpha\text{-}Nb_2C \parallel [010]Nb$. Other crystalline forms of niobium carbides, such as NbC, were detected neither in the precipitates nor in the GB segregates.

In order to determine the penetration depths of the segregated carbides inside the bulk, several cross sections were prepared by focused ion beam (FIB) milling after depositing a Pt protective layer. A cross section along the dashed line in Fig. 2(f) is given in Fig. 2(h). The dark contrast close to the surface corresponds to the segregated carbide, which extends ∼350 nm in depths and is ∼250 nm wide. This is in-line with the finding that the performance of such cavities could be recovered after a 5 μm electropolishing step. Because the carbides are larger than the London's penetration depth of 40 nm in Nb, these would resist the superconducting current. Contaminated GBs are known to form weak Josephson junctions through which the superconducting current can tunnel.[38] Due to GB contamination, the critical current of the junctions is exceeded and leads to a decoupling of the grains and hence results in a high power loss, leading to the anomalous Q-degradation observed here [Fig. 1(a), curve III].

The cold regions (#3 and #5) and the quench region (#4), located on the regular cavity area, contain fine Nb grains. A large area EBSD map over ≈5 mm^2 in the cold region is displayed in Fig. 3(a) and the corresponding grain size distribution of about 2400 detected grains in Fig. 3(b), depicting an average size of ∼43 μm. On the other hand, a much higher number of grains (approximately 3300) were detected within a ∼3.75 mm^2 area in the quench region [Fig. 3(d)] with an increasing frequency for decreasing grain size [Fig. 3(e)]. Excess of small sized (<30 μm) grains results in an increased amount of GBs in this region. A typical surface morphology of cold and quench regions, observed by means of SEM, is displayed in Figs. 3(c) and 3(f), respectively, where triangular precipitates are seen all over the surface. High-resolution EBSD maps of a selected area within the SEM micrographs from the quench region confirmed the Nb_2C segregation extending up to 500 nm in width at some GBs.

The large-area EBSD maps described in Figs. 3(a) and 3(b) were analyzed further to retrieve the distribution of misorientation angles (θ) between adjacent Nb grains [Fig. 4(a)]. An excess of low-angle GBs, with θ between 5° and 14°, and a shoulder close to 14° is evident for the quench region as compared to the cold region. For the welding zone, a distinct peak close to 14° is present for the quench region and absent for the cold region [Fig. S2(a)], with a much lower statistics though. Excess of carbon in the GBs of Ferrite was reported recently with a very high accuracy achieved in the 3D atomic mapping obtained by combining the methods of nano-beam diffraction in transmission electron microscopy and atomic probe tomography.[39] The GB segregation of carbon was found to increase with θ up to 14° (low-angle GBs), above which a strong spread was noticed because other crystallographic parameters start to play a role. Our observation of a high segregation of carbon in the quench regions, along with a concentration in low-angle GBs with θ close to 14°, is in a very good agreement with the bcc Fe-C system.

For certain misorientation angles, a coincidence site lattice (CSL) is formed by common lattice points present in both adjacent grains. The number of the lattice points in a unit cell of a CSL is designated by Σ. In the present system of the SRF Nb, distributions of CSL Σ values are given in Fig. 4(b), as detected in the quench and cold regions lying in the normal area of the cavity. An excess of Σ3 in the cold regions and of Σ41a in the quench regions is evident. Σ3 in bcc Nb is a coherent twin boundary along [111], and Σ41a is a symmetrical tilt GB along the [001] axis with a misorientation angle of 12.68°. The same was observed on the cutouts from the welding zone, with a less statistics [Fig. S2(b)]. These results suggest that Σ41a in bcc Nb might be prone to impurity segregation or lattice defects to lead a quench of the cavity, which needs further investigation and can be an interesting open question for theoretical modeling.

Combining the results obtained, we can propose the following different reasons for the observed Q-losses: After the first heat treatment (I), the cavity was electropolished before its RF test, implying no carbides to exist on the Nb surface. The observed quench at high fields can be correlated with the fine-grained (<30 μm) Nb region

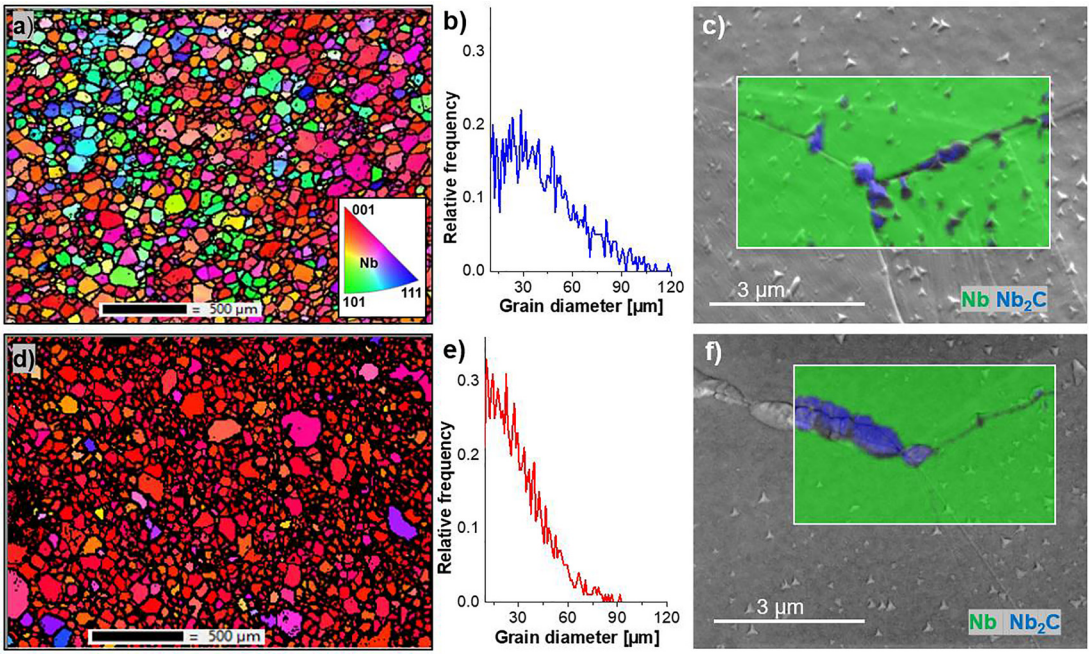

FIG. 3. Nb grain orientation maps [(a), (d)] on the cuts #3 and #4 [inset of (a): inverse pole figure of Nb]; corresponding grain size distributions [(b), (e)]; and SEM of a triple GB intersection [(c), (f)] with phase identification of Nb in green and Nb_2C in blue. The upper row corresponds to the cold region and the lower row to the quench region of cavity 1DE16.

containing a big network of low-angle GBs in high θ ($<14°$) regime, which are expected to contain a high dislocation density.[39] Such crystalline defects are known to trap remnant magnetic flux in the superconducting surface[40–42] and/or cause an early flux penetration at high RF field.[41,43,44] This is in very good agreement with the finding that a significant amount of trapped flux and a higher vacancy-cluster density were observed in this region.[18] In our case, flux trapping at cavity cooldown could be inhibited by suppressing the remnant magnetic field below 5 μT in the cavity test set-up. Therefore, an early flux penetration with increasing RF field favored by the excess low-angle grain boundaries is the most apparent cause of the observed quench.

After the second treatment (II), high Q-values were achieved up to an intermediate E_{acc} with a quench observed, the most probable loss-mechanism is due to high Ohmic losses induced by the carbides (up to 200 nm size) present on the cavity surface and most likely leading to the quench at a reduced accelerating field.

Finally, the third treatment (III) was followed without any surface removal after the second heat treatment. Carbides formed after the second heat treatment II remained in the material and so a large intake of carbon is expected as the collected carbon on the surface diffuses toward the bulk on heating to 800 °C and segregates back to the surface later on cooling down. This led to the formation of larger precipitates (>500 nm) and substantial segregation of carbides at GBs, which would decouple the flux lattice of Nb grains and, therefore, leads to the anomalous Q-degradation escalating with increasing E_{acc}. The most probable source of carbon for the formation of carbides is the residual C-content in the furnace and adventitious carbon on the cavity surface due to its exposure to the atmosphere. The impurity content of C in the starting Nb sheet material was less than 5 wt. ppm. With improved furnace conditions and chemically cleaned cavities, such strong degradation could be suppressed in the follow-up cavity treatments.[45]

From this study on the cutouts of a SRF Nb cavity, we are able to correlate: (i) the small sized Nb grain-structure with abundant low-angle GBs favoring an early flux penetration to the local superconductivity breakdown at high RF fields, (ii) Ohmic losses due to carbide

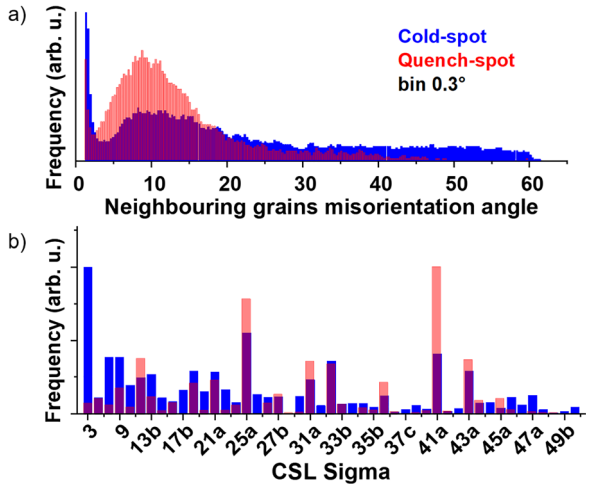

FIG. 4. (a) Distribution of mis-orientation angle θ and (b) occurrence of coincidence site lattice Σ values for the cold region #3 (blue) and quench region #4 (red).

precipitates on the cavity surface to the quench at intermediate fields, and (iii) significantly large GB segregated carbides causing flux lattice decoupling to the anomalous Q-losses starting at low fields of a few MV/m. An excess of carbide segregation on low-angle GBs in bcc Nb was also confirmed. These results emphasize the importance of grain orientation and tailor polycrystalline Nb material with preferred high-angle grain boundaries for SRF applications. Higher annealing temperatures and longer duration might be helpful to achieve this.

See the supplementary material for Figs. S1 and S2 mentioned in the text.

The annealing and testing of the Nb cavity was performed as a part of the European XFEL R&D program. This work was supported by BMBF research Grant No. 05H18GURB1. The authors acknowledge Tobias Krekeler for high resolution TEM and EDX on one sample at Technical University Hamburg.

AUTHOR DECLARATIONS

Conflict of Interest

The authors have no conflicts to disclose.

DATA AVAILABILITY

The data that support the findings of this study are available within the article and its supplementary material.

REFERENCES

[1]D. Reschke, V. Gubarev, J. Schaffran, L. Steder, N. Walker, M. Wenskat, and L. Monaco, Phys. Rev. Accel. Beams **20**, 042004 (2017).
[2]A. Vrajitoarea, Z. Huang, P. Groszkowski, J. Koch, and A. A. Houck, Nat. Phys. **16**, 211–217 (2020).
[3]S. V. Kutsaev, K. Taletski, R. Agustsson, P. Carriere, A. N. Cleland, Z. A. Conway, É. Dumur, A. Moro, and A. Y. Smirnov, EPJ Quantum Technol. **7**, 7 (2020).
[4]A. Romanenko and D. I. Schuster, Phys. Rev. Lett. **119**, 264801 (2017).
[5]A. Romanenko, R. Pilipenko, S. Zorzetti, D. Frolov, M. Awida, S. Belomestnykh, S. Posen, and A. Grassellino, Phys. Rev. Appl. **13**, 034032 (2020).
[6]W. Singer, A. Brinkmann, R. Brinkmann, J. Iversen, A. Matheisen, W.-D. Moeller, A. Navitski, D. R. J. Schaffran, A. Sulimov, N. Walker, H. Weise, P. Michelato, L. Monaco, C. Pagani, and M. Wiencek, Phys. Rev. Accel. Beams **19**, 092001 (2016).
[7]A. Grassellino, A. Romanenko, Y. Trenikhina, M. Checchin, M. Martinello, O. Melnychuk, S. Chandrasekaran, D. Sergatskov, S. Posen, A. Crawford, S. Aderhold, and D. Bice, Supercond. Sci. Technol. **30**, 094004 (2017).
[8]A. Romanenko, D. Bafia, A. Grassellino, M. Martinello, and Y. Trenikhina, in Proceedings of the 19th International Conference on RF Superconductivity SRF, THP014 (2019).
[9]P. Dhakal, S. Chetri, S. Balachandran, P. J. Lee, and G. Ciovati, Phys. Rev. Accel. Beams **21**, 032001 (2018).
[10]H. Padamsee, Supercond. Sci. Technol. **30**, 053003 (2017).
[11]H. Padamsee, *RF Superconductivity: Science, Technology and Applications*, Vol. II (Wiley-VCH Verlag GmbH and Co., KGaA, Weinheim, 2009).
[12]G. Ciovati, G. Myneni, F. Stevie, P. Maheshwari, and D. Griffis, Phys. Rev. Accel. Beams **13**, 022002 (2010).
[13]C. Z. Antione, Matériaux Tech. **91**, 45–50 (2003).
[14]G. Pfeiffer and H. Wipf, J. Phys. F **6**, 167 (1976).
[15]H. Dosch, U. Schubert, H. Metzgert, and J. Peisl, J. Phys. F **14**, 2467 (1984).
[16]T. Metzger, U. Schubert, and J. Peisl, J. Phys. F **15**, 779 (1985).
[17]G. D. L. Semione, V. Vonk, A. Dangwal Pandey, E. Grånäs, B. Arndt, M. Wenskat, W. Hillert, H. Noei, and A. Stierle, J. Phys.: Condens. Matter **33**, 265001 (2021).
[18]M. Wenskat, C. Bate, A. Dangwal Pandey, A. Jeromin, T. Keller, J. Knobloch, J. Köszegi, F. Kramer, O. Kugeler, S. Kulkarni, D. Reschke, J. Schaffran, G. D. L. Semione, S. S. An, L. Steder, A. Stierle, and N. Walker, Supercond. Sci. Technol. **33**, 115017 (2020).
[19]K. Umemori, E. Kako, T. Konomi, S. Michizono, H. Sakai, J. Tamura, and T. Okada, in 19th International Conference on RF Superconductivity SRF (2019).
[20]M. Fouaidy, F. Chatelet, D. Le Drean, D. Longuevergne, R. Martret, G. Olry, T. Pepin-Donat, T. Proslier, and L. Maurice, IEEE Trans. Appl. Supercond. **31**, 1–8 (2021).
[21]B. Aune, R. Bandelmann, D. Bloess, B. Bonin, A. Bosotti, M. Champion, C. Crawford, G. Deppe, B. Dwersteg, D. A. Edwards, H. T. Edwards, M. Ferrario, M. Fouaidy, P.-D. Gall, A. Gamp, A. Gössel, J. Graber, D. Hubert, M. Hüning, M. Juillard, T. Junquera, H. Kaiser, G. Kreps, M. Kuchnir, R. Lange, M. Leenen, M. Liepe, L. Lilje, A. Matheisen, W.-D. Möller, A. Mosnier, H. Padamsee, C. Pagani, M. Pekeler, H.-B. Peters, O. Peters, D. Proch, K. Rehlich, D. Reschke, H. Safa, T. Schilcher, P. Schmüser, J. Sekutowicz, S. Simrock, W. Singer, M. Tigner, D. Trines, K. Twarowski, G. Weichert, J. Weisend, J. Wojtkiewicz, S. Wolff, and K. Zapfe, Phys. Rev. Spec. Top. Accel. Beams **3**, 092001 (2000).
[22]T. Yegor, Ph.D. thesis, Univ. Hamburg, 2016.
[23]B. Bein, Master thesis, Univ. Hamburg, 2019.
[24]B. Schmitz, J. Köszegi, K. Alomari, O. Kugeler, and J. Knobloch, Rev. Sci. Instrum. **89**, 054706 (2018).
[25]B. Bonin and R. W. Röth, Part. Accel. **40**, 59–83 (1992).
[26]A. Grassellino, A. Romanenko, A. Crawford, O. Melnychuk, A. Rowe, M. Wong, D. Sergatskov, D. Bice, Y. Trenikhina, L. D. Cooley, C. Ginsburg, and R. D. Kephart, arXiv:1305.2182v2 (2013).
[27]C. Antoine, H. Safa, B. Berthier, and J. P. Galien, in Proceedings of the 19th International Conference on RF Superconductivity (1997).
[28]H. Noei, V. Vonk, T. F. Keller, R. Röhlsberger, and A. Stierle, J. Large-Scale Res. Facilities **2**, A76 (2016).
[29]A. Darlinski and J. Halbritter, Surf. Interface Anal. **10**, 223–237 (1987).
[30]I. Arfaouito, C. Guillot, J. Cousty, and C. Z. Antione, J. Appl. Phys. **91**, 9319 (2002).
[31]A. Dangwal Pandey, G. Dalla Lana Semione, A. Prudnikava, T. F. Keller, H. Noei, V. Vonk, Y. Tamashevich, E. Elsen, B. Foster, and A. Stierle, J. Mater. Sci. **53**, 10411–10422 (2018).
[32]M. Naguib, J. Halim, J. Lu, K. M. Cook, L. Hultman, Y. Gogotsi, and M. W. Barsoum, J. Am. Chem. Soc. **135**, 15966–15969 (2013).
[33]G. D. L. Semione, A. Dangwal Pandey, S. Tober, J. Pfrommer, A. Poulain, J. Drnec, G. Schütz, T. F. Keller, H. Noei, V. Vonk, B. Foster, and A. Stierle, Phys. Rev. Accel. Beams **22**, 103102 (2019).
[34]A. J. Wilkinson and T. B. Britton, Mater. Today **15**, 366 (2012).
[35]A. L. Giorgi, E. G. Szklarz, E. K. Storms, and A. L. Bowman, Phys. Rev. **129**, 1524 (1963).
[36]E. Rudy and C. E. Brukl, J Am. Ceram. Soc. **50**, 265–268 (1967).
[37]B. Vishwanadh, T. S. R. C. Murthy, A. Arya, R. Tewari, and G. K. Dey, J. Alloys Compd. **671**, 424 (2016).
[38]B. Bonin and H. Safa, Part. Accel. **40**, 59 (1992).
[39]M. Herbig, D. Raabe, Y. Li, P. Choi, S. Zaefferer, and S. Goto, Phys. Rev. Lett. **112**, 126103 (2014).
[40]S. Balachandran, A. Polyanskii, S. Chetri, P. Dhakal, Y.-F. Su, Z.-H. Sung, and P. J. Lee, Sci Rep **11**, 5364 (2021).
[41]C. Antoine, Phys. Rev. Accel. Beams **22**, 034801 (2019).
[42]Z.-H. Sung, M. Wang, A. A. Polyanskii, C. Santosh, S. Balachandran, C. Compton, D. C. Larbalestier, T. R. Bieler, and P. J. Lee, J. Appl. Phys. **121**, 193903 (2017).
[43]A. Romanenko, in Proceedings of the 14th International Conference on RF Superconductivity SRF (2009).
[44]A. Romanenko and H. Padamsee, Supercond. Sci. Technol. **23**, 045008 (2010).
[45]M. Wenskat, C. Bate, T. F. Keller, A. Dangwal Pandey, B. Foster, D. Reschke, J. Schaffran, G. D. L. Semione, S. Sievers, A. Stierle, N. Walker, and H. Weise, in Proceedings of LINAC 2018, Beijing, China (2018).